Available online at www.sciencedirect.com
SCIENCE DIRECT®
Journal of Solid State Chemistry 177 (2004) 4482–4493
JOURNAL OF SOLID STATE CHEMISTRY
www.elsevier.com/locate/jssc

The crystal and molecular structure of $N_2H_5[M(N_2H_3COO)_3]\cdot H_2O$ ($M\in\{Co, Zn\}$) isomorphic compounds—an X-ray crystallographic, vibrational spectroscopic and quantum-chemical study

Adolf Jesih[a], Anka Rahten[a], Primož Benkič[a], Tomaž Skapin[a], Ljupčo Pejov[b,*], Vladimir M. Petruševski[b]

[a]*Jožef Stefan Institute, Jamova 39, SI-1000 Ljubljana, Slovenia*
[b]*Institute of Chemistry, Faculty of Science, Sts. Cyril and Methodius University, P.O. Box 162, 1000 Skopje, Macedonia*

Received 17 June 2004; received in revised form 16 August 2004; accepted 19 August 2004
Available online 11 November 2004

Abstract

A systematic study of $N_2H_5[M(N_2H_3COO)_3]\cdot H_2O$ ($M\in\{Co, Zn\}$) type of compounds, which are typical model systems for transition metal complexes with α-amino acids (the latter are not obtainable in crystalline form), was carried out. The crystal structures of these compounds were solved by X-ray crystallographic methods. FTIR spectra at room and low temperature (~100 K) as well as Raman spectra at room temperature were recorded, and analyzed in details. Also, the geometries of the $Zn(N_2H_3COO)_3^-$ and $N_2H_5^+$ species were fully optimized at ab initio HF and B3LYP/6-31+G(*d*,*p*) level of theory, and subsequent vibrational analyses were performed on the basis of which several important reassignments of the IR and Raman bands were proposed. In order to study the binding energetics and the ligand–cation charge-transfer interactions within the $Zn(N_2H_3COO)_3^-$ complex, NBO analysis was carried out, employing the second-order perturbation theory analysis of the Fock matrix (i.e., its Kohn–Sham analog) within the NBO basis.

Keywords: Amino acid complexes; Hydrazidocarbonate complexes; Hydrazidocarbonic acid; Hydrazinium cation; Crystal structure; FTIR spectra; Raman spectra; Vibrational analysis; NBO analysis; ab initio HF and DFT methods

1. Introduction

Hydrazidocarbonic acid, N_2H_3COOH and its hydrazinium salt, $N_2H_5(N_2H_3COO)$ were first isolated in 1904 by Stollé and Hoffman [1]. Hydrazidocarbonates appear in six different types, where besides a central cation and hydrazidocarbonato groups, K^+, $N_2H_5^+$, N_2H_4 and H_2O can be found [2–6].

These compounds are very interesting in contemporary materials science as precursors for the preparation of potentially useful materials. Thermal decomposition of $N_2H_5[M(N_2H_3COO)_3]\cdot H_2O$ (M = Fe, Co, Ni), $Cu(N_2H_3COO)_2\cdot 0.5H_2O$ and $Co(N_2H_3COO)_2$ in inert or reductive atmosphere leads to the corresponding metals in the form of very reactive powders [7]. By thermal decomposition/combustion at 523 K in air atmosphere, a finely dispersed α-Fe_2O_3 was prepared from $Fe(N_2H_3COO)_2\cdot 2N_2H_4$ and $N_2H_5[Fe(N_2H_3COO)_3]\cdot H_2O$ precursors [8]. α-Fe_2O_3 doped with Co was made from solid solutions of $N_2H_5[Co_xFe_{1-x}(N_2H_3COO)_3]\cdot H_2O$, ($x = 1-10$ at%) [9] and Mn–Zn ferrites, suitable as materials for high speed magnetic tapes, and transformer cores, were prepared from the $(N_2H_5)_3[Mn_xZn_{1-x}Fe_2(N_2H_3COO)_9]\cdot 3H_2O$ ($x = 0.2-0.8$) [9]. Hydrazidocarbonates may be used as precursors for the formation of cobaltites [10] and manganites [11] as well. The advantage of these

*Corresponding author. Fax: +389-2-3226-865.
E-mail address: ljupcop@iunona.pmf.ukim.edu.mk (L. Pejov).

0022-4596/$ - see front matter © 2004 Published by Elsevier Inc.
doi:10.1016/j.jssc.2004.08.033

precursors is the low temperature at which they are decomposed into metals or oxide powders. Decomposition temperatures depend on the properties of the central cations and autocatalytic and exothermic behavior of the hydrazine and hydrazinium ions [12]. Decomposition is accompanied by the evolution of a considerable amount of gases with the consequent formation of fine particles with a large surface area.

On the other hand, the mentioned complexes are of significant importance in biochemical research, since they may serve as model systems for the amino-acid complexes with transition metals that cannot be obtained in the crystalline form [13–15]. Namely, it has been recognized that the structures of hydrazidocarbonate complexes are very similar to the structures of the corresponding complexes of α-amino-acids [13–15] with divalent metal cations.

Infrared spectra on hydrazidocarbonates are scarce and incomplete [16] and there are essentially no Raman vibrational data on this type of compounds. Also, to the best of our knowledge, no ab initio force field data have been presented for this type of metal complexes.

In this paper, we report a systematic study of the $N_2H_5[M(N_2H_3COO)_3]\cdot H_2O$ (M = Zn, Co) compounds by X-ray crystallography, FTIR and Raman spectroscopy as well as with quantum chemical modelling.

2. Experimental and computational details

2.1. Synthesis

ZnO (99%, Riedel de Haen) or $CoCl_2\cdot 6H_2O$ (B.D.H. Ltd. Poole) were dissolved in a 10% water solution of $N_2H_4\cdot H_2O$ (B.D.H. Ltd. Poole) saturated with gaseous CO_2. By the additional introduction of CO_2 into solutions for 3 days two compounds were isolated, namely $N_2H_5[Zn(N_2H_3COO)_3]\cdot H_2O$ and $N_2H_5[Co(N_2H_3COO)_3]\cdot H_2O$ [17–19], respectively. The samples were dried over H_2SO_4 in a desiccator.

2.2. Vibrational spectroscopy

Infrared spectra at room temperature (RT) in the range 400–4000 cm^{-1} were recorded on a Perkin–Elmer FTIR 1710 spectrometer as both Nujol and fluorolube mulls pressed between CsBr and NaCl windows. Both room and low-temperature (LT ≈ 100 K) FTIR spectra were recorded on a Perkin–Elmer System 2000 FTIR. The working instrument resolution was 4 cm^{-1}, and 128 spectra were accumulated and averaged for the LT measurements in order to improve the signal-to-noise ratio. Averaging of 64 spectra was sufficient to obtain satisfactory signal-to-noise ratio at RT. A Graseby-Specac variable temperature cell was used for the low temperature measurements.

Raman spectra were recorded on a dispersion Raman instrument Renishaw Ramascope, System 1000. As excitation source the 632.8 nm He–Ne laser line was used. Raman spectra were recorded in the range 100–4000 cm^{-1} using 25 mW power excitation line. By using a 50× microscope objective the laser beam was focused onto a spot of approximately 1 in diameter, and the collected scattered light was passed through a spectrophotometer onto a CCD detector.

2.3. X-ray crystallography

For both $N_2H_5[Zn(N_2H_3COO)_3]\cdot H_2O$ and $N_2H_5[Co(N_2H_3COO)_3]\cdot H_2O$ crystals all X-ray crystallographic measurements were made on a Rigaku AFC7S diffractometer with graphite monochromatic Mo $K\alpha$ radiation at a temperature of 20(1) °C. Further basic crystallographic details are given in Table 1. Both structures were solved by direct methods [20] and expanded using Fourier techniques. After refinement of all non-hydrogen atoms including anisotropic displacement parameters against all reflections [21], the positions of hydrogen atoms were localized in a Fourier difference map and finally refined with isotropic temperature factor. Absolute configurations of the models were checked with Flack parameter [22], which for both present models converged to zero.

2.4. Quantum chemical calculations

Full geometry optimizations of both the $Zn(NH_2NHCOO)_3^-$ anionic complex and of the NH_2–NH_3^+ cation were performed at both the Hartree-Fock (HF) and the Density functional (DFT) levels of theory, using Schlegel's gradient optimization algorithm by computing the energy derivatives with respect to nuclear coordinates analytically [23]. Within the DFT-based methodology, a combination of Becke's three-parameter hybrid adiabatic connection exchange functional (B3, [24]) with the Lee-Yang-Parr correlation functional (LYP, [25])—B3-LYP was employed. Let us also briefly recall that B3LYP is in fact a hybrid HF-DFT approach [24–26]. Namely, Becke's three-parameter adiabatic connection exchange functional is of the form [24–26]:

$$AE_X^{Slater} + (1-A)E_X^{HF} + B\Delta E_X^{Becke88} + E_C^{VWN} + C\Delta E_C^{nonlocal}, \quad (1)$$

where the constants A, B and C have been determined by fitting to the G1 set of molecules. Obviously, it contains an admixture of the HF exchange, in contrast to the "pure DFT" methodologies. It has been found that the hybrid DFT methodology based on the B3-LYP combination of functionals is the method of choice for prediction of a large number of molecular properties

Table 1
The basic crystallographic data for $N_2H_5[Co(N_2H_3COO)_3]\cdot H_2O$ and $N_2H_5[Zn(N_2H_3COO)_3]\cdot H_2O$

Empirical formula	$C_3CoH_{16}N_8O_7$		$C_3H_{16}N_8O_7Zn$
Formula weight	335.17		341.61
Crystal color, habit	Violet, prism		Colorless, prism
Crystal dimensions	$0.4\times0.3\times0.35$ mm		$0.5\times0.45\times0.4$
Crystal system		Monoclinic	
Lattice type		C-centered	
Lattice parameters	$a = 12.139(2)$ Å		$a = 12.127(7)$ Å
	$b = 10.916(3)$ Å		$b = 10.914(2)$ Å
	$c = 10.261(2)$ Å		$c = 10.301(3)$ Å
	$\beta = 120.92(2)^\circ$		$\beta = 120.94(2)^\circ$
	$V = 1166.4(4)$ Å^3		$V = 1169.4(7)$ Å^3
Space group		*Cc* (No.9)	
Z value		4	
D_{calc}	1.909 g/cm^3		1.940 g/cm^3
F_{000}	692.00		704.00
Radiation		Mo*K*α ($\lambda = 0.71069$ Å)	
μ(Mo*K*α)	1.522 mm^{-1}		2.152 mm^{-1}
Temperature		20.0 °C	
θ_{max}	30.0°		32.5°
Scan width	$(1.42+0.35\tan\theta)^\circ$		$(1.52+0.35\,tan\,\theta)^\circ$
No. of reflections measured	Total: 6654		Total: 8318
	Unique: 3411 ($R_{int} = 0.012$)		Unique: 4258 ($R_{int} = 0.031$)
No. of observations ($I > 2.00\sigma(I)$)	3339		4179
PSI absorbtion correction	trans. fact: 0.530–0.629		trans. factors: 0.358–0.422
Secondary extinction coefficient[a]	0.0084(5)		0.0216(9)
Flack parameter	0.002(7)		0.002(4)
Refinement		Full-matrix least-squares against all F^2	
No. of variables	235		235
R_1; wR_2;	0.0171; 0.0447		0.0192; 0.0512
R_1(all); wR_2(all)	0.0179; 0.0451		0.0197; 0.0516
Goodness of fit indicator	1.030		1.023
Max peak in final diff. map	0.20 (4) e_0/Å^3		0.26(5) e_0/Å^3
Min peak in final diff. map	−0.20(4) e_0/Å^3		−0.20(5) e_0/Å^3

[a] $F_c^* = kF_c[1+0.001\times F_c^2\lambda_3/\sin(2\theta)]^{-1/4}$; *x*—extinction parameter, *k*—overall scale factor.

[27–30 and references therein]. The "fine grid" (75, 302) was used for numerical integration (75 radial and 302 angular integration points) in all DFT calculations. The standard Pople-style 6-31 + G(*d*,*p*) basis set, including a diffuse *sp* shell on all heavy atoms, was used for orbital expansions in solving both the HF and the Kohn–Sham (KS) SCF equations. Subsequent to the geometry optimizations, harmonic vibrational analyses were performed for the stationary points found on the molecular potential energy hypersurfaces (PESs) in order to test their characters and to obtain the harmonic vibrational frequencies and normal modes. The absence of imaginary frequencies (negative eigenvalues of the Hessian matrices) confirmed that the stationary points found by the optimization procedures correspond to real minima, instead of being saddle points.

Since the cobalt anionic complex—$Co(NH_2NHCOO)_3^-$ contains an odd number of electrons, due to convergence problems with the UHF and UKS algorithms (it was necessary to use the quadratically convergent—QC SCF algorithm in each step), quantum chemical calculations for this system were prohibitively expensive.

In order to obtain information on the binding forces between the Zn^{2+} cation and the NH_2NHCOO^- anionic ligands, a natural bond orbital (NBO) analysis of the anionic cluster was carried out, employing also the second-order perturbation theory analysis of the Fock matrix (i.e. its Kohn–Sham analog) within the NBO basis [31–36].

All quantum chemical calculations were performed with Gaussian98 series of programs [37].

3. Results and discussion

3.1. Structures

The compounds $N_2H_5[Zn(N_2H_3COO)_3]\cdot H_2O$ and $N_2H_5[Co(N_2H_3COO)_3]\cdot H_2O$ appeared to be isostructural, as is often the case. They crystallize in the monoclinic space group *Cc* (no. 9) with four formula units in the unit cell and are also isostructural with the

compound $N_2H_5[Ni(N_2H_3COO)_3]\cdot H_2O$ [38]. The basic crystallographic data for the two compounds are summarized in Table 1. Positional and equivalent isotropic displacement parameters for both compounds are given in Table 2 (the anisotropic displacement parameters for both compounds may be obtained from the authors upon request), while selected interatomic distances and angles are given in Tables 3 and 4.

The structures consist of one chelate anion ($M^{II}(N_2H_3COO)_3^-$, M = Zn, Co) of an octahedral type with a defined conformation, O1, O3, O5 and N1, N3, N5 atoms of the N_2H_3COO acting as bidentate ligand groups and lying on the opposite triangular faces of the octahedra (Fig. 1).

Angles between bonds, formed between coordinating atoms, metal center and neighboring atoms in the chelate ligand, are close to 116° on atoms O1, O3, O5, while for the N1, N3 and N5 ones the values are around 107°. On the basis of the natural hybrid orbital concept [31–36], one can attribute such geometric features to the basic type of hybridization on the neighboring C1, C2, C3 and N2, N4, N6 atoms (almost sp^2 and sp^3, respectively). M^{II}–O distances are shorter than M^{II}–N. In the case of the Zn(II) complex, this is due to the much more pronounced charge-transfer interaction from carboxyl group oxygen atom to the central Zn^{2+} cation, than from the NH_2 group nitrogen atom to the cation. On the basis of the NBO analysis, this is elaborated in more detail in Section 3.2.

The present structures are characterized by relatively strong hydrogen bonds [39] of the N–H···O, O–H···O and also N–H···N type. The N–H and O–H distances show the usual systematic shortening as observed by X-ray methods, so hydrogen bonding interactions were searched for in the limit of sum of van der Waals radii for acceptor and donor atom ($r_O^W + r_N^W + r_H^W \cong 3.2$ Å).

Table 2
Atomic coordinates and isotropic displacement factors for $N_2H_5[Co(N_2H_3COO)_3]\cdot H_2O$ and $N_2H_5[Zn(N_2H_3COO)_3]\cdot H_2O$

	x/a		y/b		z/c		$U_{eq}(U_{iso})10^4/Å^2$	
Atom	Co	Zn	Co	Zn	Co	Zn	Co	Zn
Co/Zn	0.4989	0.5036	0.424603(12)	0.424188(9)	0.5005	0.5024	187.6(5)	222.9(4)
O1	0.37338(10)	0.37704(9)	0.54236(10)	0.54147(9)	0.32805(11)	0.32783(10)	240(2)	263(2)
O2	0.17684(11)	0.18017(10)	0.62308(11)	0.62237(11)	0.21535(14)	0.21556(14)	364(3)	388(2)
O3	0.64962(10)	0.65341(9)	0.48153(9)	0.48362(9)	0.47341(11)	0.47303(10)	247(2)	272(2)
O4	0.79733(10)	0.80129(9)	0.62829(9)	0.63031(9)	0.53714(13)	0.53811(12)	292(2)	314(2)
O5	0.44790(11)	0.45447(10)	0.27188(9)	0.27226(9)	0.36500(11)	0.36506(10)	287(2)	321(2)
O6	0.49222(14)	0.49570(16)	0.07299(9)	0.07253(8)	0.36306(17)	0.36400(18)	362(3)	390(2)
O7	0.48194(12)	0.48511(11)	0.77492(12)	0.77467(11)	0.31554(14)	0.31703(13)	334(2)	358(2)
N1	0.32676(12)	0.32996(11)	0.40644(11)	0.40758(10)	0.51167(13)	0.51338(12)	222(2)	247(2)
N2	0.22995(11)	0.23351(10)	0.47890(12)	0.47993(11)	0.39332(15)	0.39477(13)	275(2)	296(2)
N3	0.57092(13)	0.57658(12)	0.57822(10)	0.57832(8)	0.65119(14)	0.65409(12)	225(2)	247(2)
N4	0.68003(12)	0.68467(10)	0.62541(11)	0.62603(9)	0.65034(14)	0.65177(12)	250(2)	272(2)
N5	0.62407(13)	0.62770(11)	0.28912(12)	0.28664(11)	0.66231(14)	0.66446(12)	267(2)	297(2)
N6	0.61224(15)	0.61499(14)	0.18307(12)	0.18126(12)	0.57541(16)	0.57730(14)	363(3)	384(2)
N7	0.91940(13)	0.92262(11)	0.40286(12)	0.40245(12)	0.51992(17)	0.52048(14)	273(2)	304(2)
N8	0.86638(13)	0.86973(11)	0.29160(12)	0.29114(12)	0.54148(16)	0.54270(14)	295(2)	325(2)
C1	0.26224(12)	0.26603(10)	0.55261(12)	0.55240(10)	0.31063(14)	0.31134(12)	209(2)	230(2)
C2	0.70853(13)	0.71240(11)	0.57711(10)	0.57837(9)	0.54697(15)	0.54766(14)	210(2)	236(2)
C3	0.51143(13)	0.51544(11)	0.17474(12)	0.17435(11)	0.42734(16)	0.42792(14)	245(2)	275(2)
H11	0.309(2)	0.318(3)	0.331(2)	0.338(3)	0.500(3)	0.505(4)	410(60)	560(80)
H12	0.335(2)	0.336(4)	0.432(2)	0.431(3)	0.600(3)	0.600(5)	270(50)	490(90)
H2	0.161(2)	0.166(3)	0.485(2)	0.491(3)	0.398(3)	0.399(3)	360(50)	520(70)
H31	0.514(2)	0.513(2)	0.628(2)	0.633(3)	0.619(3)	0.625(3)	370(50)	360(50)
H32	0.593(2)	0.601(3)	0.561(2)	0.565(2)	0.745(2)	0.743(3)	230(40)	320(60)
H4	0.695(2)	0.698(2)	0.698(2)	0.706(2)	0.674(3)	0.672(3)	340(50)	290(40)
H51	0.698(3)	0.703(3)	0.315(3)	0.310(3)	0.713(3)	0.713(3)	590(80)	410(60)
H52	0.600(2)	0.606(3)	0.268(2)	0.268(3)	0.726(2)	0.729(3)	280(50)	370(60)
H6	0.644(2)	0.645(3)	0.120(2)	0.121(3)	0.627(3)	0.619(3)	410(60)	400(60)
H71	0.921(3)	0.795(4)	0.397(2)	0.278(5)	0.442(4)	0.477(5)	480(70)	780(120)
H72	1.000(3)	0.887(3)	0.404(2)	0.282(3)	0.591(3)	0.633(4)	480(70)	580(80)
H73	0.873(2)	0.919(4)	0.472(2)	0.403(4)	0.515(2)	0.434(5)	290(50)	660(100)
H81	0.779(3)	0.999(4)	0.311(3)	0.401(3)	0.475(4)	0.582(5)	660(90)	590(80)
H82	0.884(3)	0.876(2)	0.291(2)	0.469(2)	0.635(3)	0.518(3)	510(70)	320(50)
H91	0.450(3)	0.461(3)	0.705(3)	0.701(3)	0.318(3)	0.314(4)	610(80)	540(70)
H92	0.429(3)	0.437(3)	0.799(2)	0.793(3)	0.233(3)	0.235(4)	460(60)	560(80)

$U_{eq} = 1/3(U_{11}(aa^*)^2 + U_{22}(bb^*)^2 + U_{33}(cc^*)^2 + 2U_{12}(aa^*bb^*)\cos\gamma + 2U_{13}(aa^*cc^*)\cos\beta + 2U_{23}(bb^*cc^*)\cos\alpha)$.

Table 3
Interatomic distances in $N_2H_5[Co(N_2H_3COO)_3]\cdot H_2O$ and $N_2H_5[Zn(N_2H_3COO)_3]\cdot H_2O$ (crystallographically determined), together with the HF and B3LYP/6-31+G(*d*,*p*) values for the $N_2H_5^+$ and $Zn(N_2H_3COO)_3^-$ species

	Co (experimental)	Zn (experimental)	HF	B3LYP
M–O1	2.082(1)	2.095(1)	2.011	2.039
M–O3	2.082(1)	2.092(1)	2.011	2.039
M–O5	2.052(1)	2.059(1)	2.011	2.039
M–N1	2.160(1)	2.174(2)	2.398	2.337
M–N3	2.140(1)	2.152(1)	2.398	2.337
M–N5	2.156(1)	2.173(2)	2.398	2.337
O1–C1	1.271(2)	1.273(2)	1.258	1.281
O2–C1	1.257(2)	1.259(1)	1.213	1.236
N1–N2	1.419(2)	1.420(2)	1.397	1.419
N2–C1	1.365(2)	1.366(2)	1.420	1.445
O3–C2	1.271(2)	1.268(1)	1.258	1.281
O4–C2	1.263(2)	1.266(1)	1.213	1.236
N3–N4	1.425(2)	1.422(2)	1.397	1.419
N4–C2	1.378(2)	1.380(2)	1.420	1.445
O5–C3	1.273(2)	1.271(1)	1.258	1.281
O6–C3	1.251(2)	1.251(2)	1.213	1.236
N5–N6	1.423(2)	1.418(2)	1.397	1.419
N6–C3	1.380(2)	1.386(2)	1.420	1.445
N7–N8	1.444(2)	1.446(2)	1.425	1.449
N7–H71	0.82(3)	0.87(4)	1.011	1.028
N7–H72	0.87(3)	0.81(4)	1.011	1.028
N7–H73	0.92(2)	0.92(2)	1.013	1.033
N8–H81	0.94(3)	0.81(4)	1.002	1.020
N8–H82	0.87(3)	0.84(3)	1.002	1.020
N1–H11	0.84(3)	0.77(4)	1.003	1.021
N1–H12	0.90(2)	0.89(4)	0.999	1.016
N2–H2	0.86(2)	0.85(3)	0.998	1.016
N3–H31	0.81(2)	0.90(3)	1.003	1.021
N3–H32	0.88(2)	0.82(3)	0.999	1.016
N4–H4	0.82(3)	0.89(2)	0.998	1.016
N5–H51	0.81(3)	0.82(3)	1.003	1.021
N5–H52	0.88(2)	0.86(3)	0.999	1.016
N6–H6	0.83(3)	0.76(3)	0.998	1.016
O9–H91	0.87(3)	0.85(3)		
O9–H92	0.80(3)	0.77(3)		

Table 4
Interatomic angles in $N_2H_5[Co(N_2H_3COO)_3]\cdot H_2O$ and $N_2H_5[Zn(N_2H_3COO)_3]\cdot H_2O$ (crystallographically determined), together with the HF and B3LYP/6-31+G(*d*,*p*) values for the $N_2H_5^+$ and $Zn(N_2H_3COO)_3^-$ species

Angle (see Fig. 1)	Co (experimental)	Zn (experimental)	HF	B3LYP
O1–M–O3	90.67(4)	89.65(4)	110.2	107.6
O1–M–O5	95.25(4)	94.41(4)	110.2	107.6
O1–M–N1	78.26(4)	78.10(5)	73.1	75.3
O1–M–N3	88.81(5)	89.54(5)	84.2	82.7
O1–M–N5	174.39(5)	173.62(4)	161.9	166.8
O3–M–O5	97.57(4)	96.68(4)	110.2	107.6
O3–M–N1	167.20(4)	165.88(4)	161.9	166.8
O3–M–N3	78.56(4)	78.41(4)	73.1	75.3
O3–M–N5	89.29(5)	90.88(5)	84.2	82.7
O5–M–N1	89.90(5)	91.30(5)	84.2	82.7
O5–M–N3	174.45(5)	173.71(4)	161.9	166.8
O5–M–N5	79.20(5)	79.21(5)	73.1	75.3
N1–M–N3	94.64(5)	94.31(5)	89.9	92.6
N1–M–N5	102.37(5)	102.08(5)	89.9	92.6
N3–M–N5	96.68(5)	96.80(5)	89.9	92.6
M–O1–C1	115.71(8)	115.44(7)	125.4	122.4
M–O3–C2	115.51(8)	115.24(7)	125.4	122.4
M–O5–C3	116.24(9)	116.11(8)	125.4	122.4
M–N1–N2	107.56(8)	107.48(7)	105.0	105.8
M–N3–N4	108.35(8)	108.22(7)	105.0	105.8
M–N5–N6	105.73(8)	105.49(8)	105.0	105.8
N1–N2–C1	118.97(11)	119.13(10)	117.3	116.7
O1–C1–O2	123.67(12)	123.60(11)	128.5	128.5
O1–C1–N2	118.93(11)	119.28(10)	116.0	116.2
O2–C1–N2	117.30(12)	117.01(11)	115.4	115.1
N3–N4–C2	117.90(11)	118.03(9)	117.3	116.7
O3–C2–O4	123.95(12)	123.77(11)	128.5	128.5
O3–C2–N4	118.95(12)	119.46(10)	116.0	116.2
O4–C2–N4	117.01(12)	116.68(11)	115.4	115.1
N5–N6–C3	119.38(12)	119.75(11)	117.3	116.7
O5–C3–O6	125.01(14)	125.11(13)	128.5	128.5
O5–C3–N6	117.64(12)	117.80(11)	116.0	116.2
O6–C3–N6	117.31(13)	117.04(13)	115.4	115.1

The strongest interactions are given in Table 5. It can be seen that both of the carboxyl group oxygen atoms of the ligand act as hydrogen-bond proton acceptors. Non-coordinated carboxyl oxygen atom O2 is the acceptor for hydrogen bonds where donors are non-coordinated $N4^4$ atom from ligand N_2H_3COO and $N7^2$ atom from $N_2H_5^+$ cation, while O4 atom forms strong hydrogen bonds where donors are coordinated $N1^3$ atom from ligand molecule and N7 atom from $N_2H_5^+$ cation. O4 atom also accepts hydrogen bond from uncoordinated water molecule. The same water molecule also acts as a hydrogen-bond proton donor to the coordinated carboxyl atom O1 from neighboring chelate anion. O6 atom participates in one strong hydrogen bond with non-coordinated $N2^3$ atom as a proton donor. Additionally, $O6^3$ and $O9^3$ atoms are involved in bifurcated hydrogen bond that is donated by N7 atom from cation $N_2H_5^+$. In that way all three hydrogen atoms from N7 atom of $N_2H_5^+$ cation participate in hydrogen bonds, while N8 atom from the same cation donates one hydrogen bond to coordinated $O5^4$ atom from ligand molecule and accepts one hydrogen bond from coordinated N3 atom at a ligand molecule. In chelate anion coordinated O1 and O3 atoms are also acceptors of hydrogen bonds from coordinated $N1^2$ and $N3^2$ atoms, respectively. Non-coordinated N6 atom from ligand molecule donates slightly weaker hydrogen bond to N2 atom what must be the consequence of packing (Fig. 1), which is mostly driven by interactions between cation $N_2H_5^+$ and chelate anion $M^{II}(N_2H_3COO)_3^-$ (M=Zn, Co), where also strongest hydrogen bonds are formed. Chelate anions are additionally connected by strong hydrogen bonds donated by uncoordinated water molecule.

The minima located on HF and B3LYP/6-31+G(*d*,*p*) PESs of the free $Zn(NH_2NHCOO)_3^-$ anion and the free

$N_2H_5^+$ cation are presented in Figs. 2 and 3. The computed bond lengths and angles are compared with the X-ray data in Tables 3 and 4. As can be seen, the agreement between theory and experiment is very good, the B3LYP values being significantly superior over the HF ones for almost all structural parameters, especially the *M*–O and *M*–N distances within the coordination sphere. The agreement between theoretical quantum chemical predictions and X-ray experimental data may be considered as very satisfactory especially having in mind that the QM geometry optimizations are performed for free molecular/ionic species (in vacuum, at 0 K), while experimental crystallographic data refer to species "packed" in a crystal surrounding (i.e.,

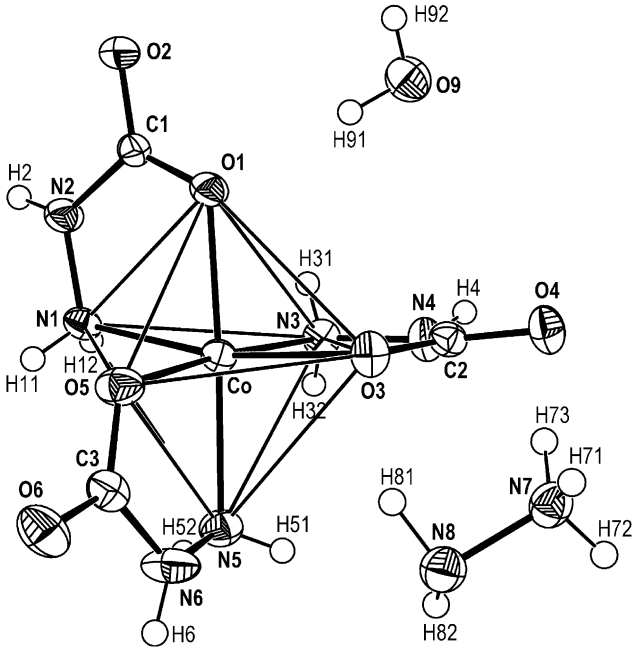

Fig. 1. The crystal structure of $N_2H_5[Co(N_2H_3COO)_3]\cdot H_2O$.

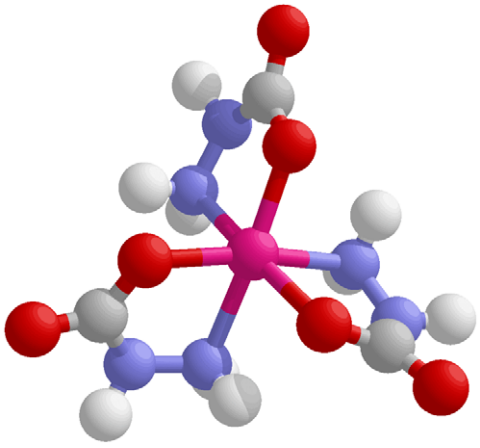

Fig. 2. The optimized geometry of $Zn(N_2H_3COO)_3^-$ anion at B3LYP/6-31 + G(*d*,*p*) level of theory.

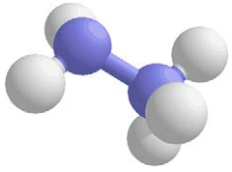

Fig. 3. The optimized geometry of $N_2H_5^+$ cation at B3LYP/6-31 + G(*d*,*p*) level of theory.

Table 5
The hydrogen bonding network in $N_2H_5[Co(N_2H_3COO)_3]\cdot H_2O$ and $N_2H_5[Zn(N_2H_3COO)_3]\cdot H_2O$ (crystallographically determined)

Type of H-bond	$N_2H_5[Co(N_2H_3COO)_3]\cdot H_2O$		$N_2H_5[Zn(N_2H_3COO)_3]\cdot H_2O$	
X–H⋯*Y* (*X*, *Y* = N, O)	Distance *X*–*Y* (Å)	Angle *X*–H⋯*Y* (deg)	Distance *X*–*Y* (Å)	Angle *X*–H⋯*Y* (deg)
N1–H11⋯O4[3]	3.084	164.5	3.071	167.8
N1–H12⋯O1[2]	3.047	168.0	3.037	169.1
N2–H2⋯O6[3]	2.925	154.6	2.915	160.1
N3–H31⋯N8[3]	3.160	173.0	3.170	170.8
N3–H32⋯O3[2]	3.004	178.3	2.995	175.5
N4–H4⋯O2[4]	2.830	163.5	2.831	163.1
N5–H52⋯O9[2]	2.954	161.2	2.952	159.2
N7–H73⋯O4	2.924	170.3	2.942	170.2
N7–H72⋯O2[2]	2.725	166.8	2.723	172.3
N7−H71⋯O6[3]	2.878	117.8	2.880	121.1
N7−H71⋯O9[3]	2.926	143.0	2.923	134.0
N8–H82⋯05[4]	3.017	160.4	3.009	162.3
O9–H92⋯O4[4]	2.778	175.0	2.777	167.9
O9–H91⋯O1	2.893	178.5	2.891	165.3

Symmetry operations used for generatinq equivalent atoms: [2]: $x, -y, z+1/2$; [3]: $x+1/2, y+1/2, z$; [4]: $x+1/2, -y+1/2, z+1/2$.

immersed in a crystal field), and also taking part into various intermolecular interactions with the neighboring species, such as the H-bonding interactions. Still, as stated by Boese et al. [40], the ab initio calculated minima on molecular potential energy hypersurfaces may be very valuable in rationalizing, or even verifying, the X-ray structural data. It is important to note within this context that effective core potential basis sets are quite inappropriate for studying such chelate systems, as our preliminary HF/LANL2DZ studies have shown. When such methodology is employed, the agreement between theory and experiment is significantly poor.

3.2. NBO analysis

In order to judge, at least semiquantitatively, on the main binding forces in the case of the Zn-ligand interaction, we have performed an NBO analysis of the $Zn(NH_2NHCOO)_3^-$ anionic complex. Specifically, the NBO analysis provides information on the magnitude and direction of the charge-transfer interactions within the cluster. The NBO analysis was based on the B3LYP/6-31 + G(*d*,*p*) density as this level of theory was found to be much more reliable than the HF one, for both geometry optimization, as well as for the harmonic vibrational analyses.

First, we have performed a second-order perturbation theory analysis of the Fock matrix, or, more precisely, its Kohn–Sham analog, within the NBO basis (Table 6). As revealed by this analysis, by far the most significant charge transfer (CT) between the monomeric units within this anionic cluster is from the anionic hydrazidocarbonate ligands to the central Zn^{2+} cation. This charge transfer occurs predominantly from the two non-bonding orbitals centered on carboxylate oxygen atom (the oxygen atom lone pairs) of each anionic ligand to the Zn^{2+} 4*s* orbital ($n \rightarrow 4s$), and from the nitrogen atom non-bonding orbital (the nitrogen atom lone pair) of each ligand to the Zn^{2+} 4*s* orbital (again, $n \rightarrow 4s$). Also, rather smaller CT occurs between the bonding (σ) C–O and N–H orbitals from each ligand to the Zn^{2+} 4*s* orbital ($\sigma \rightarrow 4s$) as well as from a 1*s* core orbital of carboxylate group oxygen atom of each ligand to the Zn^{2+} 4*s* orbital ($1s \rightarrow 4s$) and from the non-bonding orbital centered on carboxylate oxygen of each anionic ligand to a Zn^{2+} Rydberg state ($n \rightarrow Ry^*$). The only significant back-donation from the central Zn^{2+} cation occurs from the Zn^{2+} 4*s* orbital to the antibonding (σ^*) C–O orbital of each anionic ligand ($4s \rightarrow \sigma^*$). The only significant CT interaction between the ligands themselves takes place from the non-bonding orbital centered on carboxylate oxygen of each ligand to the

Table 6
Results from the second-order perturbation theory analysis of the Kohn–Sham analog of the Fock matrix within the NBO basis at B3LYP/6-31 + G(*d*,*p*) level of theory for the $Zn(NH_2NHCOO)_3^-$ anionic complex

Donor orbital	Acceptor orb.	$\Delta E^{(2)}$/(kcal mol^{-1})	$(E_{acc} - E_{don})$/a.u.	$\langle\psi^*_{don}\|\hat{F}\|\psi_{acc}\rangle$/a.u.	$q_{don.\rightarrow acc.}/e$
$n^{(1)}$ (O^A)	4*s*(Zn)	38.2	0.37	0.11	0.177
$n^{(1)}$ (O^B)	4*s*(Zn)	38.2	0.37	0.11	0.177
$n^{(1)}$ (O^C)	4*s*(Zn)	38.2	0.37	0.11	0.177
n (N^A)	4*s*(Zn)	24.5	0.40	0.10	0.125
n (N^B)	4*s*(Zn)	24.5	0.40	0.10	0.125
n (N^C)	4*s*(Zn)	24.5	0.40	0.10	0.125
$n^{(2)}$ (O^A)	4*s*(Zn)	13.9	0.66	0.09	0.037
$n^{(2)}$ (O^B)	4*s*(Zn)	13.9	0.66	0.09	0.037
$n^{(2)}$ (O^C)	4*s*(Zn)	13.9	0.66	0.09	0.037
σ (C–O^A)	4*s*(Zn)	3.4	0.99	0.06	0.007
σ (C–O^B)	4*s*(Zn)	3.4	0.99	0.06	0.007
σ (C–O^C)	4*s*(Zn)	3.4	0.99	0.06	0.007
1*s* (O^A)	4*s*(Zn)	2.5	18.91	0.22	0.0003
1*s* (O^B)	4*s*(Zn)	2.5	18.91	0.22	0.0003
1*s* (O^C)	4*s*(Zn)	2.5	18.91	0.22	0.0003
$n^{(1)}$ (O^A)	*Ry**(Zn)	2.2	1.46	0.05	0.002
$n^{(1)}$ (O^B)	*Ry**(Zn)	2.2	1.46	0.05	0.002
$n^{(1)}$ (O^C)	*Ry**(Zn)	2.2	1.46	0.05	0.002
σ (N–H^A)	4*s*(Zn)	1.6	0.70	0.03	0.004
σ (N–H^B)	4*s*(Zn)	1.6	0.70	0.03	0.004
σ (N–H^C)	4*s*(Zn)	1.6	0.70	0.03	0.004
4*s*(Zn)	σ^* (C–O^A)	1.1	0.49	0.04	0.013
4*s*(Zn)	σ^* (C–O^B)	1.1	0.49	0.04	0.013
4*s*(Zn)	σ^* (C–O^C)	1.1	0.49	0.04	0.013
$n^{(1)}$ (O^A)	σ^* (N–H^B)	0.9	0.70	0.02	0.002
$n^{(1)}$ (O^B)	σ^* (N–H^C)	0.9	0.70	0.02	0.002
$n^{(1)}$ (O^C)	σ^* (N–H^A)	0.9	0.70	0.02	0.002

N–H antibonding orbital of the neighboring ligand ($n \rightarrow \sigma^*$).

The estimated energetic effects due to these interactions are given by the second-order perturbation theoretical expressions of the form [31–36]:

$$\Delta E^{(2)}_{\psi_{\text{donor}} \rightarrow \psi_{\text{acceptor}}} \approx -2 \frac{\langle \psi^*_{\text{don}} | \hat{F} | \psi_{\text{acc}} \rangle^2}{\varepsilon_{\text{acc}} - \varepsilon_{\text{don}}}, \quad (2)$$

where ε_i is a diagonal NBO matrix element of the Fock operator $\hat{F}$, or, more rigorously, the Kohn–Sham one-electron analog $\hat{h}_{\text{KS}}$. All the NBO parameters related to the outlined discussion are given in Table 6.

The quantities of transferred charge from a given donor to a given acceptor orbital may be estimated again using elementary perturbation theory arguments, leading to the following approximate formula:

$$q_{\psi_{\text{donor}} \rightarrow \psi_{\text{acceptor}}} \approx 2 \left(\frac{\langle \psi^*_{\text{don}} | \hat{F} | \psi_{\text{acc}} \rangle}{\varepsilon_{\text{acc}} - \varepsilon_{\text{don}}} \right)^2. \quad (3)$$

The calculated values for $Zn(NH_2NHCOO)_3^-$ anionic complex are also given in Table 6. Obviously, the magnitude of transferred charge within the cluster is quite relevant from the stabilization aspect, especially having in mind that it has been emphasized that even seemingly small values of transferred charge (0.001–0.01e) lead to chemically significant stabilization energies [31–36].

3.3. Vibrational analysis

The LT FTIR spectra and the RT Raman spectra of the studied compounds are presented in Fig. 4. As can be seen, the structural isomorphism between the cobalt and zinc compounds is evident also from their spectra.

The experimentally observed vibrational frequencies together with the HF and B3LYP/6-31+G(d,p) harmonic values and the approximate descriptions of the normal modes are given in Tables 7 and 8. The computed raw values of harmonic vibrational frequencies were scaled by the factors proposed by Scott and Radom [41] in order to account, at least partially, for the systematic errors inherent to quantum-mechanical vibrational analyses.

The symmetry operators for the isolated $Zn(NH_2NHCOO)_3^-$ anionic complex, generate the following vibrational irreducible representations within the point group C_3:

$$\Gamma_{\text{vib.}} = 23A \oplus 23E.$$

All the fundamental modes for this complex are thus expected to be both IR and Raman active. On the other hand, for the C_s minimum on the cationic $N_2H_5^+$ potential energy hypersurface, the vibrational reducible representation decomposes as

$$\Gamma_{\text{vib.}} = 9A' \oplus 6A''.$$

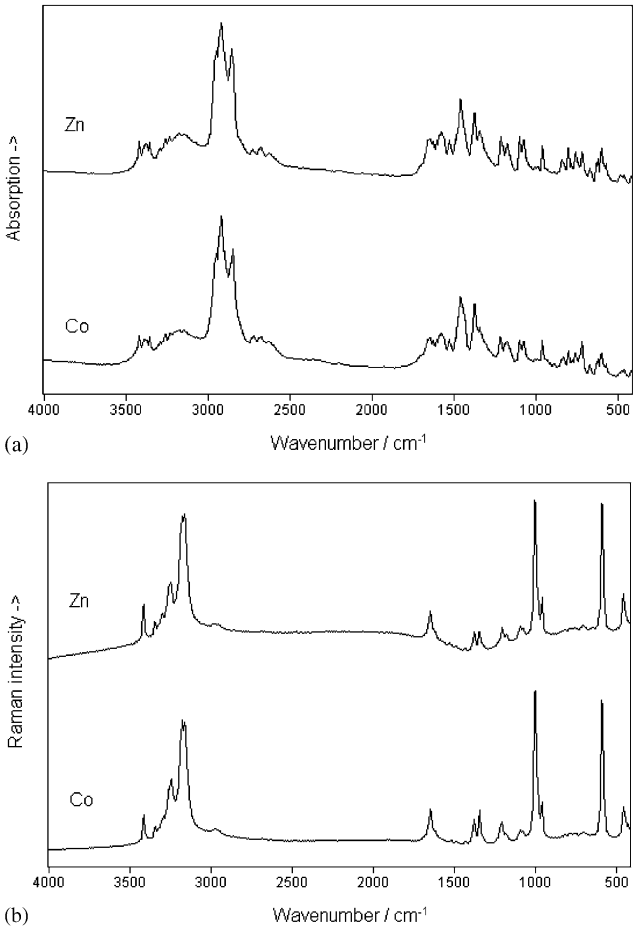

Fig. 4. (a) LT FT IR spectra and (b) RT Raman spectra of $N_2H_5[Zn(N_2H_3COO)_3] \cdot H_2O$ and $N_2H_5[Co(N_2H_3COO)_3] \cdot H_2O$.

All vibrational modes being again both IR and Raman active.

However, the site-symmetries of both species in the crystal are C_1, while the point group isomorphic to the factor group is C_s. The unit-cell group analysis for the $N_2H_5^+$ and $Zn(NH_2NHCOO)_3^-$ species is presented in Fig. 5. Since the quantum chemical calculations refer to isolated species, the symmetry of normal modes given in Tables 7 and 8 is that generated by the symmetry operators of the "free molecule" point group.

3.3.1. The N–N stretching modes

In the literature, considerable attention has been paid to the region of appearance of bands due to the N–N stretching mode in the IR spectra of hydrazine and its derivatives [16,17,42]. As it has been already pointed out, upon protonation of hydrazine, this band shifts to higher frequencies, due to diminution of the repulsion between two lone pairs in the parent molecule. In the present case, the ν(N−N) band in the case of $M(NH_2NHCOO)_3^-$ anion appears at higher frequency

Table 7
The HF and B3LYP/6-31 + G(*d*,*p*) harmonic vibrational frequencies of the $Zn(N_2H_3COO)_3^-$ anion, together with the experimental LT FTIR values for $N_2H_5[Zn(N_2H_3COO)_3]\cdot H_2O$ and $N_2H_5[Co(N_2H_3COO)_3]\cdot H_2O$

B3LYP		HF		Sym.	Experimental		Approximate description
ν/cm^{-1}	I/km mol^{-1}	ν/cm^{-1}	I/km mol^{-1}		ν/cm^{-1} (Zn)	ν/cm^{-1} (Co)	
3434.6	9.1	3440.9	16.7	*A*	3379	3381	$\nu^{asym}(NH_2)$
3433.9	7.0	3440.4	11.2	*E*			$\nu^{asym}(NH_2)$
3409.5	5.0	3436.0	16.0	*E*	3351	3351	ν(NH)
3409.2	4.9	3436.0	6.2	*A*			ν(NH)
3311.5	9.7	3339.1	2.5	*A*	3235	3228	$\nu^{sym}(NH_2)$
3310.9	1.8	3338.5	5.0	*E*			$\nu^{sym}(NH_2)$
1691.2	64.3	1724.7	75.8	*A*	1580	1581	$\nu^{asym.}(COO) + \delta(NH)$
1670.5	1184.0	1700.9	1470.8	*E*			$\nu^{asym}(COO) + \delta(NH)$
1613.3	27.1	1642.8	59.9	*A*	1633	1634	$\delta^{sciss}(NH_2)$
1612.5	13.0	1642.9	16.3	*E*			$\delta^{sciss.}(NH_2)$
1363.5	31.5	1431.8	99.6	*A*	1366	1365	δ(NH)
1362.7	44.6	1429.7	76.4	*E*			δ(NH)
1302.9	417.6	1353.8	572.8	*A*	1384	1383	$\nu^{sym.}(COO) + \delta(NH) + \nu(CN)$
1289.1	163.6	1341.1	188.9	*E*	1343	1344	$\nu^{sym.}(COO) + \delta(NH) + \nu(CN)$
1238.1	1.6	1271.5	3.5	*E*	1239	1240	$\delta^{twist.}(NH_2)$
1236.7	3.5	1272.0	1.5	*A*			$\delta^{twist.}(NH_2)$
1102.3	27.2	1153.5	20.3	*E*	1009	1008	$\nu(NN)$
1101.1	16.9	1152.8	0.4	*A*	994	995	$\nu(NN)$
976.7	58.8	1023.3	78.7	*A*	1081	1083	$\delta^{wagg.}(NH_{2)+\delta(NH2)})$
972.2	205.6	1017.1	284.7	*E*	1075	1077	$\delta^{wagg.}(NH_{2)+\delta(NH2)})$
891.7	89.1	930.5	60.0	*E*	841	839	$\nu(CN) + \delta^{wagg.}(NH_2)$
889.7	98.0	931.1	116.0	*A*			$\nu(CN) + \delta^{wagg.}(NH_2)$
770.9	120.0	823.9	177.1	*A*	805	803	τ(HNCO)
766.7	18.4	819.9	50.4	*E*			τ(HNCO)
737.5	25.4	755.5	20.5	*E*	785	784	τ(HNNH)
731.3	123.6	751.3	150.5	*A*	758	760	τ(HNNH)
609.1	72.3	623.8	62.9	*A*	667	669	$\delta^{rock.}(NH_2)$
605.9	20.7	622.8	20.8	*E*			$\delta^{rock.}(NH_2)$
554.2	5.5	569.2	2.7	*A*			δ(ring)
546.7	4.7	561.8	5.9	*E*			δ(ring)
502.2	103.4	491.9	114.5	*A*	485	480	$\delta^{rock.}(NH_2) + \gamma$(NH)
455.2	29.5	443.9	31.7	*E*			$\delta^{rock.}(NH_2) + \gamma$(NH)
364.4	28.4	363.8	35.7	*A*			ν(ZnN) + δ(CNN)
359.7	9.9	360.1	12.5	*E*			ν(ZnN) + δ(CNN)
251.7	91.9	255.6	105.0	*E*			ν(ZnO)
223.5	13.5	216.7	11.6	*A*			ν(ZnO)

than the corresponding band due to the $NH_2NH_3^+$ cation. The bands appearing at 994 and 1009 cm^{-1} in the LT FTIR spectra of the Zn compound and at 995 and 1008 cm^{-1} in the case of the Co one are attributed to the unit cell group components of the ν(N−N) stretching band due to the NH_2NHCOO^- ligand. On the other hand, the band appearing at 963 cm^{-1} in the case of $N_2H_5Zn(N_2H_3COO)_3\cdot H_2O$ and at 966 cm^{-1} in the cobalt analog may be attributed to the ν(N−N) stretching band due to the non-coordinated $N_2H_5^+$ species. This trend is also predicted by ab initio harmonic force field calculations. In the present case, further blue shift of the ν(N−N) mode in comparison to the $NH_2NH_3^+$ species may be attributed to the delocalization of the lone pair of the nitrogen center bonded to the carboxylic group. This standpoint is supported by the fact that the –NHCOO fragment is planar and the geometry around the carbon atom corresponds closely to expectations based on sp^2 hybridization. The delocalization thus exhibits a more pronounced diminution of the interaction between the lone pairs in the hydrazine derivatives in comparison to the protonation itself. However, ab initio results are not in quantitative agreement with the experimental data. As can be seen from Table 8, the calculated frequency of the ν(N−N) mode due to $NH_2NH_3^+$ species is lower by more than 100 cm^{-1} than the experimental value. Much of this disagreement may be attributed to the fact that within the crystal, the $NH_2NH_3^+$ cations act as hydrogen-bond proton acceptors, due to the remaining lone pair on the NH_2 group nitrogen atom. Such interaction, engaging the remaining lone pair is expected to lead to a

Table 8
The HF and B3LYP/6-31+G(*d*,*p*) harmonic vibrational frequencies of the $N_2H_5^+$ cation, together with the experimental LT FTIR values for $N_2H_5[Zn(N_2H_3COO)_3]\cdot H_2O$ and $N_2H_5[Co(N_2H_3COO)_3]\cdot H_2O$

B3LYP		HF		sym.	Experimental		Approximate description
ν/cm^{-1}	$I/km\,mol^{-1}$	ν/cm^{-1}	$I/km\,mol^{-1}$		ν/cm^{-1} (Zn)	ν/cm^{-1} (Co)	
3448.5	74.7	3453.8	94.8	A''	3421	3421	$\nu^{asym.}(NH_2)$
3344.4	46.8	3351.0	56.1	A'	3291	3292	$\nu^{sym.}(NH_2)$
3326.5	133.4	3326.6	154.8	A''	3259	3259	$\nu^{asym.}(NH_3)$
3299.6	110.7	3315.0	131.8	A'	3179	3179	$\nu^{asym.}(NH_3)$
3201.7	22.3	3227.3	42.7	A'	3140	3140	$\nu^{sym.}(NH_3)$
1634.9	6.8	1645.8	5.5	A'	1644	1644	$\delta(NH_2)+\delta(NH_3)$—out of phase
1607.4	43.6	1621.3	47.0	A''	1625	1624	$\delta^{asym.}(NH_3)$
1595.7	76.1	1609.7	77.5	A'	1605	1605	$\delta(NH_2)+\delta(NH_3)$—in phase
1513.9	83.9	1538.9	113.6	A'	1526	1527	$\delta^{sym.}(NH_3)$—umbrella
1377.3	16.1	1394.4	16.6	A''	1377	1377	$\delta^{wagg.}(NH_2)+\delta^{wagg.}(NH_3)$—in phase
1145.2	1.9	1159.0	1.7	A'			$\delta^{asym.}(NH_3)$
1023.3	95.7	1030.6	71.9	A'	1098	1097	$\delta(NH_2)+\delta(NH_3)$—out of phase
1019.6	15.8	1021.4	17.4	A''			$\delta^{wagg.}(NH_2)+\delta^{wagg.}(NH_3)$—out of phase
834.7	111.5	880.1	150.7	A'	963	966	$\nu(N-N)+\delta(NH_2)$
322.5	51.2	298.3	52.7	A''			$\tau(NH_2-NH_3)$

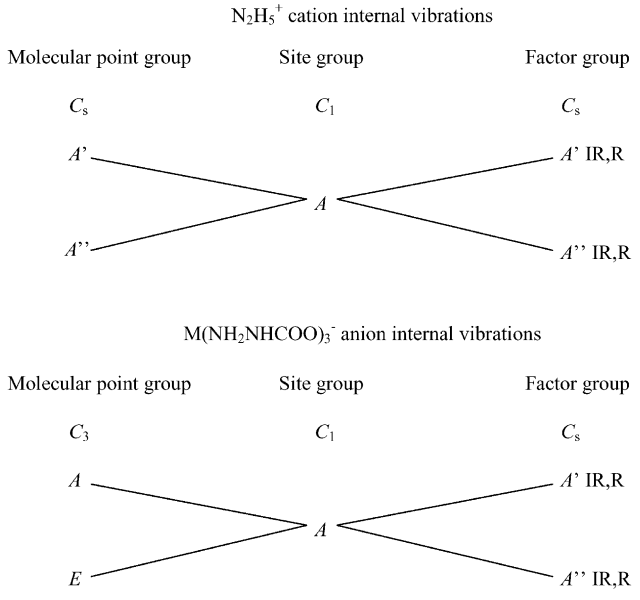

Fig. 5. The unit-cell group analysis for the $N_2H_5^+$ and $Zn(NH_2NHCOO)_3^-$ species.

further blue shift of the ν(N−N) mode as compared to the free $NH_2NH_3^+$ species. Besides that, it is also worth reminding once again that theoretical results refer to an isolated cation/anion species. "In-crystal" situation is much more complex; the crystalline field, further modified by interactions of the Davydov type, considerably affects the vibrational force field of the studied species. The quantitative agreement is thus unexpected for the studied case. In the Raman spectra, the ν(N−N) modes due to the $M(NH_2NHCOO)_3^-$ and $NH_2NH_3^+$ species give rise to two bands at 960 and 1006 cm^{-1}, respectively. It should be noted that the Raman scattering activity ratio of these two bands shows an opposite trend in comparison to the IR intensity ratio.

3.3.2. The COO stretching modes

Regarding the carboxylate group stretching modes in this type of compounds, only scarce literature data exist on their assignment [17,43,44]. According to these purely empirical assignments, the band appearing at $\approx$1610 cm^{-1} in the IR spectra of $N_2H_5[Zn(N_2H_3COO)_3]\cdot H_2O$ and $N_2H_5[Co(N_2H_3COO)_3]\cdot H_2O$ should be attributed to the antisymmetric COO stretching mode, while the one at $\approx$1390 cm^{-1} is due to the symmetric COO stretching mode. The separation between the two bands is $\approx$220 cm^{-1}. However, our present results, based on both the HF and B3LYP/6-31+G(*d*,*p*) force fields, especially the predicted IR intensities of the corresponding bands strongly suggest that the bands appearing at 1580 cm^{-1} in the case of Zn compound and at 1581 cm^{-1} in cobalt analog should be attributed to the antisymmetric COO stretching vibration. On the other hand, the symmetric COO stretch should be expected to appear at about 1300 cm^{-1} (for the free $Zn(N_2H_3COO)_3^-$ anion) and should also be the most intense band in this spectral region. It thus seems that the bands appearing at 1384 and 1343 cm^{-1} in the case of $N_2H_5[Zn(N_2H_3COO)_3]\cdot H_2O$ and at 1383 and 1344 cm^{-1} in the case of $N_2H_5[Co(N_2H_3COO)_3]\cdot H_2O$ may be safely attributed to vibrations of structurally different anion moieties (these would correspond to unit-cell group components of this mode, if the structure was one of higher symmetry, so the real situation may be somewhere between these two extremes) in contrast to the previous purely empirical assignments.

It is important to note within this context, and with respect to the chosen methodology, that the HF/LANL2DZ vibrational analysis based on effective core potential description of core electrons suggests that the mode which includes the symmetric COO stretching should appear at higher frequencies than the mode which is predominantly antisymmetric COO vibration. This method is, however, of much lesser reliability.

3.3.3. The NH, NH_2 and NH_3 stretching and bending modes

The NH stretching and bending modes in this type of compounds have also been only scarcely discussed and the assignments proposed so far are only empirical. Namely, the situation is quite complex, since these modes arise from both the $M(NH_2NHCOO)_3^-$ and $NH_2NH_3^+$ species. Also, the investigated compounds are hydrates, and water stretching and bending modes appear in the same spectral regions. According to ab initio HF and DFT force fields, the antisymmetric NH_2 stretching mode due to $NH_2NH_3^+$ cation should appear at highest frequency among all the NH stretching modes. Then, the antisymmetric NH_2 stretching modes within the $M(NH_2NHCOO)_3^-$ species (A and E components) and the NH stretch should follow. Such prediction may be in fact rationalized in terms of the natural hybrid orbital concept. In most general form, the sp^λ hybrid orbitals have the form:

$$h_\lambda(\theta) = N(s + \lambda^{1/2} p_\theta),$$

where p_θ is a normalized p orbital pointing in the direction θ, N is the normalization constant, while λ may be non-integer in general. The "best" such hybrid orbitals for a given molecular system may be related to the molecular geometry, as has been thoroughly discussed [31–36]. Since the hydrazidocarbonate anion coordinates to the metal cation through the NH_2 group nitrogen atom, the NH bonds are formed from the sp^λ hybrids with more pronounced p character compared to the NH bonds of the NH_2 group within the $NH_2NH_3^+$ species, which "contains" a lone pair on nitrogen. The force constant of the NH_2 stretching modes in the last case is thus expected to be larger even on the basis of such simple reasoning.

The NH_2 symmetric stretching vibrations of the $NH_2NH_3^+$ cation are expected to be blue-shifted in comparison to the A and E components of the $\nu_{sym}(NH_2)$ of $M(NH_2NHCOO)_3^-$. Finally, the antisymmetric and symmetric NH_3 stretching modes localized within $NH_2NH_3^+$ are expected to appear at lowest frequencies. Thus, even without an account for the site and unit-cell group splitting of these modes, 11 bands are expected to appear in the ν(NH) spectral region. Having in mind that the NH, NH_2 and NH_3 stretching potential may be significantly modified as a result of the hydrogen bonding interactions, a possible increase in the vibrational anharmonicity would further complicate the situation.

Regarding the NH, NH_2 and NH_3 deformation modes for the studied systems, also only empirical assignments have been proposed so far [17]. According to these assignments, the NH_2 wagging mode should appear at $\approx 1350\,cm^{-1}$, while the bands appearing at $\sim$1230, 1200 and $1100\,cm^{-1}$ should be attributed to the NH_2 rocking modes. On the basis of ab initio DFT force field, the $\delta(NH_2)$ and $\delta(NH_3)$ out-of-phase vibration within the $NH_3NH_2^+$ entity should appear at about $1635\,cm^{-1}$, while the $\delta_{scissoring}(NH_2)$ mode within the $M(NH_2NHCOO)_3^-$ anion should appear at about $1610\,cm^{-1}$. Also, the antisymmetric $\delta(NH_3)$ mode of the $NH_2NH_3^+$ cation, would be expected to appear at about $1607\,cm^{-1}$, while the in-phase $\delta(NH_2)$ and $\delta(NH_3)$ vibration should appear at $\approx 1600\,cm^{-1}$. All of these bands would thus be expected to be heavily overlapped with the band corresponding to the bending modes of crystalline water. The symmetric $\delta(NH_3)$ umbrella deformation mode is expected to appear at around $1510\,cm^{-1}$. As can be seen from Fig. 4 and Tables 7 and 8, the predicted DFT spectral pattern in this region is in rather good agreement with the experimental data, and the DFT force field-based assignments of these bands is given in Tables 7 and 8.

The shoulder appearing at about $1366\,cm^{-1}$ is attributed to the δ(NH) mode of the $M(NH_2NHCOO)_3^-$ anionic entities.

On the basis of ab initio HF and DFT vibrational analyses, a substantially different order of appearance of bands due to the lower-frequency librational modes of the NH_2 and NH_3 fragments in the studied compounds than the empirically proposed one is obtained. Also, a much more exact assignment of the corresponding bands is enabled on the basis of such theoretical analyses. Thus, the rather intense band at about $1377\,cm^{-1}$ is attributed to the in-phase wagging deformation within the $NH_3NH_2^+$ cation. The order of appearance of the NH librational modes from $M(NH_2NHCOO)_3^-$ anion is: twisting (at about $1240\,cm^{-1}$), wagging (at about $1080\,cm^{-1}$) and rocking (at about 670 and $490\,cm^{-1}$). See Tables 7 and 8 for more details.

4. Conclusion

The crystal structures of isomorphic $N_2H_5[Zn(N_2H_3COO)_3]\cdot H_2O$ and $N_2H_5[Co(N_2H_3COO)_3]\cdot H_2O$ compounds were determined by X-ray crystallographic methods. Vibrational spectra (infrared and Raman) of these compounds were recorded and analysed in detail. On the basis of quantum-chemical HF and B3LYP/6-31 + G(d,p) vibrational analyses of the cationic and anionic entities constituting the studied compounds,

several important reassignments of IR and Raman bands were proposed. The reasons behind the particular order of appearance of bands in the vibrational spectra of these compounds were discussed in terms of natural bond orbital concepts. On the basis of the second-order perturbation theory analysis of the Fock matrix (i.e. its Kohn–Sham analog) within the NBO basis, conclusions about the magnitude and direction of charge-transfer interactions within the $Zn(N_2H_3COO)_3^-$ complex anion were derived.

References

[1] R. Stollé, K. Hoffman, Chem. Ber. 37 (1904) 4523.
[2] J. Maček, A. Rahten, Thermochim. Acta 144 (1989) 257.
[3] M. Maria Amala Sekar, K.C. Patil, Mat. Res. Bull. 28 (1993) 485.
[4] J. Maček, R. Hrovat, B. Novosel, J. Thermal Analysis 40 (1993) 335.
[5] H. Funk, A. Eichoff, G. Giesder, Omagia Raluca Ripan, Edit. Rep. Soc. Romania (1966) 245.
[6] I.V. Gogorošvili, M.V. Karkarašvili, L.D. Cicišvili, Ž. Neorg. Himii 1 (1956) 2753.
[7] A. Braibanti, G. Bigliardi, A.M. Manotti Lanfredi, A. Tiripicchio, Nature 211 (1966) 1174.
[8] P. Ravindranathan, K.C. Patil, J. Mat. Sci. Lett. 5 (1986) 221.
[9] K. Suresh, G.V. Mahesh, K.C. Patil, J. Thermal Anal. 35 (1989) 1137.
[10] P. Ravindranathan, G.V. Mahesh, K.C. Patil, J. Solid State Chem. 66 (1987) 20.
[11] N. Arul Dhas, K.C. Patil, J. Solid State Chem. 102 (1993) 440.
[12] A. Rahten, J. Maček, B. Novosel, Thermochim. Acta 258 (1995) 135.
[13] A. Braibanti, A.M. Manotti Lanfredi, M.A. Pellinghelli, A. Tiripicchio, Acta Crystallogr. B 27 (1971) 2448.
[14] A. Braibanti, A.M. Manotti Lanfredi, M.A. Pellinghelli, A. Tiripicchio, Acta Crystallogr. B 27 (1971) 2261.
[15] F. Bigoli, A. Braibanti, A. Tiripicchio, M. Tiripicchio Camellini, Chem. Comm. 155 (1970) 120.
[16] A. Braibanti, F. Dallavale, M.A. Pellinghelli, E. Leporati, Inorg. Chem. 7 (1968) 1430.
[17] K.C. Patil, R. Soundarajan, E.P. Goldberg, Synth. React. Inorg. Met.—Org. Chem. 13 (1983) 29.
[18] J. Slivnik, A. Rihar, B. Sedej, Monatsh. Chem. 98 (1967) 200.
[19] J. Slivnik, A. Rihar, Monatsh. Chem. 103 (1972) 1572.
[20] A. Altomare, G. Cascarano, C. Giacovazzo, A. Guagliardi, SIR92, J. Appl. Crystallogr. 26 (1993) 343–350.
[21] G.M. Sheldrick, SHELX97 (Release 97-2), Institüt für Anorganische Chemie der Universität, Tammanstrasse, vol. 4, D-3400 Göttingen, Germany, 1998.
[22] H.D. Flack, Acta Crystallogr. A 39 (1983) 876–881;
G. Bernardinelli, H.D. Flack, Acta Crystallogr. A 41 (1985) 500–511.
[23] H.B. Schlegel, J. Comp. Chem. 3 (1982) 214.
[24] A.D. Becke, Phys. Rev. A 38 (1988) 3098.
[25] C. Lee, W. Yang, R.G. Parr, Phys. Rev. B 37 (1988) 785.
[26] J.M. Seminario, P. Politzer, Modern Density Functional Theory: A Tool for Chemistry, Elsevier, 1995 (Chapters 1–4).
[27] Lj. Pejov, Chem. Phys. Lett. 339 (2001) 269.
[28] Lj. Pejov, Chem. Phys. Lett. 358 (2002) 368.
[29] Lj. Pejov, Chem. Phys. 285 (2002) 177.
[30] Lj. Pejov, K. Hermansson, J. Chem. Phys. 119 (2003) 313.
[31] L.A. Curtiss, D.J. Pochatko, A.E. Reed, F. Weinhold, J. Chem. Phys. 82 (1985) 2679.
[32] A.E. Reed, F. Weinhold, J. Chem. Phys. 83 (1985) 1736.
[33] J.P. Foster, F. Weinhold, J. Am. Chem. Soc. 102 (1980) 7211.
[34] A.E. Reed, F. Weinhold, J. Chem. Phys. 78 (1983) 4066.
[35] A.E. Reed, F. Weinhold, L.A. Curtiss, D.J. Pochatko, J. Chem. Phys. 84 (1986) 5687.
[36] A.E. Reed, R.B. Weinstock, F. Weinhold, J. Chem. Phys. 83 (1985) 735.
[37] M.J. Frisch, G.W. Trucks, H.B. Schlegel, G.E. Scuseria, M.A. Robb, J.R. Cheeseman, V.G. Zakrzewski, J.A. Montgomery, R.E. Stratmann, J.C. Burant, S. Dapprich, J.M. Millam, A.D. Daniels, K.N. Kudin, M.C. Strain, O. Farkas, J. Tomasi, V. Barone, M. Cossi, R. Cammi, B. Mennucci, C. Pomelli, C. Adamo, S. Clifford, J. Ochterski, G.A. Petersson, P.Y. Ayala, Q. Cui, K. Morokuma, D.K. Malick, A.D. Rabuck, K. Raghavachari, J.B. Foresman, J. Cioslowski, J.V. Ortiz, B.B. Stefanov, G. Liu, A. Liashenko, P. Piskorz, I. Komaromi, R. Gomperts, R.L. Martin, D.J. Fox, T. Keith, M.A. Al-Laham, C.Y. Peng, A. Nanayakkara, C. Gonzalez, M. Challacombe, P.M.W. Gill, B.G. Johnson, W. Chen, M.W. Wong, J.L. Andres, M. Head-Gordon, E.S. Replogle, J.A. Pople, Gaussian98 (Revision A.11), Gaussian, Inc., Pittsburgh, PA, 1998.
[38] A. Braibanti, A.M. Manotti Lanfredi, A. Tiripicchio, Z. Kristal. 124 (1967) 335.
[39] J. Emsley, J. Chem. Soc. Rev. 9 (1980) 91.
[40] R. Boese, T. Hanmann, P. Stellberg, Adv. Mol. Struct. Res. 1 (1995) 201.
[41] A.P. Scott, L. Radom, J. Phys. Chem. 100 (1996) 16502.
[42] S. Milićev, J. Maček, Spectrochim. Acta A 41 (1985) 651.
[43] K.C. Patil, R. Soundarajan, V.R. Pai Verneker, Proc. Ind. Acad. Sci. 88 (1979) 211.
[44] A. Braibanti, F. Dallavalle, A. Tiripicchio, Ric. Sci. 36 (1966) 1156.